Theoretical Investigations on Thermal Rearrangement Reactions of (Aminomethyl)silane

Yongming Yu[†,‡] and Shengyu Feng*[,†]

School of Chemistry and Chemical Engineering, Shandong University, Jinan 250100, P. R. China, and School of Chemistry and Chemical Engineering, Qingdao University, Qingdao 266071, P. R. China

Received: August 23, 2006; In Final Form: September 14, 2006

Thermal rearrangement reactions of (aminomethyl)silane $H_3SiCH_2NH_2$ were studied by ab initio calculations at the G3 level. The results show that two dyotropic reactions could happen when $H_3SiCH_2NH_2$ is heated. In one reaction, the silyl group migrates from the carbon to the nitrogen atom while a hydrogen atom shifts from the nitrogen to the carbon atom, forming (methylamino)silane CH_3NHSiH_3 (reaction A). This reaction can proceed via three paths: a path involving two consecutive steps with two transition states and one intermediate metastable carbene species (A-1); and two concerted paths (A-2 and A-3). In the other reaction, the amino group migrates from the carbon to the silicon atom while a hydrogen atom shifts from the silicon to the carbon atom, via a double three-membered ring transition state, forming aminomethylsilane CH_3SiH_2-NH_2 (reaction B). Reaction rate constants, changes ($\Delta S^{\ddagger}$, ΔH, and ΔG) in thermodynamic functions and equilibrium constants of the reactions were calculated with the MP2(full)/6-311G(d,p) optimized geometries, harmonic vibrational frequencies and G3 energies of reactants, transition states, intermediates and products with statistical mechanical methods and the conventional transition-state theory (TST) with Wigner tunneling approximation over a temperature range 400−1800 K.

1. Introduction

Studies on rearrangement reactions of (aminomethyl)silanes under either strong base[1] or free radical-initiating conditions[2,3] have been reported since the 1970s. In 1974, Brook[1] and co-workers reported that under strong base conditions, (aminomethyl)trimethylsilanes can undergo 1,2 anionic rearrangement, in which the trimethylsilyl group migrates from the carbon to the nitrogen atom, and form (methylamino)trimethylsilanes (Scheme 1). They found that a phenyl group makes the

SCHEME 1

$$R_3SiCHR'NHR'' \overset{\text{base}}{\rightleftharpoons} R_3SiNR''CH_2R'$$

rearrangement more rapid when it is connected to the central carbon atom, whereas the reaction can hardly happen when it is attached to the nitrogen atom. In 1993, through a series of NMR studies on $[Me_3SiCHR^1-NR^2]^{\bullet}$, Harris and Waltonhe[2,3] observed the [1,2] migration of the trimethylsilyl radical from carbon to nitrogen atoms and suggested that the reaction occurs via a three-membered-ring transition state (Scheme 2) in which

SCHEME 2

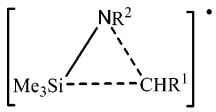

Transition state

silicon is pentacoordinate. However, Roberts and Vazquez-Persaudin[4] believe that it is more likely that the reactions proceed via an elimination−addition path (Scheme 3). Later on, Schiesser and Styles's[5] ab initio investigations on (aminomethyl)silane radical $[H_3SiCH_2NH]^{\bullet}$ lend support to Harris' model. Up to now, however, to our knowledge, no reports on thermal rearrangement reactions of (aminomethyl)silanes are available, despite the fact that (aminoalkyl)organosilicon compounds or polymers play important roles[6] in modifications of organic polymers with the aid of the reaction activity of the aminoalkyl groups, to endow the organic polymers with the excellent properties of the polysiloxanes. For this application, however, thermal decomposition or rearrangement is a disadvantage. Therefore, understanding their decomposition or rearrangement conditions and mechanisms is of practical value for the control and application of these compounds. In this paper, high level ab initio studies on thermal rearrangement reactions of (aminomethyl)silane, $H_3SiCH_2NH_2$ and the analysis of its kinetic and thermodynamic properties will be reported.

SCHEME 3

$$Me_3SiCHR^1-\dot{N}R^2 \rightleftharpoons Me_3\dot{S}i + CHR^1{=}NR^2 \rightleftharpoons R^1\dot{C}H-N(R^2)SiMe_3$$

2. Theoretical Methods

Optimized geometries for the stationary points were located using the second-order Møller−Plesset theory[7] at the MP2(full)/6-31G(d) and MP2(full)/6-311G(d,p) levels. To verify whether the stationary points are local minima or first-order saddle points, the corresponding harmonic vibrational frequencies were calculated at the same levels. Energies of stationary points were obtained at the G3[8] level. The reaction paths were examined by intrinsic reaction coordinate (IRC) calculations at the MP2-(full)/6-31G(d) level. A natural bond orbital (NBO)[9] analysis was performed at the MP2(full)/6-311G(d,p) level. All calculations were carried out using the Gaussian 03 revision C02 series of programs.[10] Reaction rate constants ($k(T)$), changes ($\Delta S^{\ddagger}$, ΔH,

* To whom correspondence should be addressed. E-mail: fsy@sdu.edu.cn. Fax: 86-531-88564464.
† Shandong University.
‡ Qingdao University.

10.1021/jp065454i CCC: $33.50
Published on Web 10/20/2006

SCHEME 4

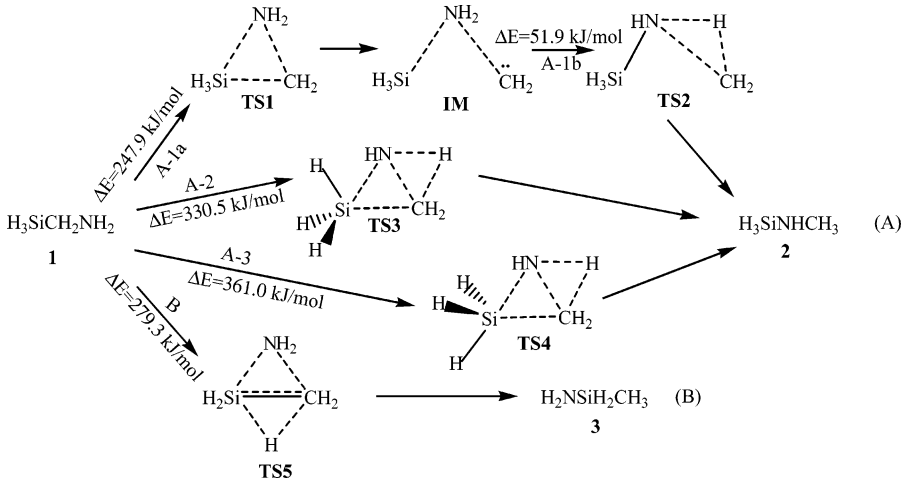

and ΔG) in thermodynamic functions and equilibrium constants of the reactions were calculated by using the MP2(full)/6-311G(d,p) optimized geometries, harmonic vibrational frequencies and G3 energies of reactants, transition states, intermediates and products with statistical mechanical methods[11] and the conventional transition-state theory (TST)[12−17] over the temperature range 400−1800 K. The rate constant is given by

$$k(T) = \frac{k_B T}{h} \frac{Q^{\ddagger}}{Q} \exp\left(\frac{-\Delta H^{\ddagger}}{RT}\right)$$

where k_B and h are the Boltzmann and Planck constants, respectively, $\Delta H^{\ddagger}$ is the activation enthalpy of the reaction, and the $Q^{\ddagger}$ and Q are the molecular partition functions of the transition state and reactant, respectively. Torsional modes of transition states were identified by direct inspection of low-frequency modes and treated as hindered internal rotations using the method of hindered rotor approximation with the RO scheme and the SC level.[18] To account for quantum mechanical tunneling effects associated with hydrogen transfer reactions, the transmission coefficients $W(T)$ were calculated using Wigner perturbation theory[19]

$$W(T) = 1 + \frac{1}{24}\left(1.44 \frac{\nu_i}{T}\right)^2$$

wherein ν_i is the magnitude of the imaginary frequency in cm^{-1} corresponding to the reaction coordinate at the transition state and T is the temperature in Kelvin. Thus the rate constants with Wigner tunneling approximation is given as

$$k_{TST/W}(T) = k(T) \times W(T)$$

In the present study all kinetic calculations were performed using POLYRATE 9.0 program.[20]

3. Results and Discussion

Two dyotropic[21] thermal rearrangements (rearrangements involving simultaneous or consecutive migration of two σ-bonds) can occur when (aminomethyl)silane $H_3SiCH_2NH_2$ (**1**) is heated (see Scheme 4). In one reaction, the migration of the silyl group from the carbon to the nitrogen atom is coupled to a migration of a hydrogen atom from the nitrogen to the carbon atom, forming (methylamino)silane CH_3NHSiH_3 (**2**) (reaction A). This reaction can proceed via three paths: a path involving two consecutive steps with two transition states and one intermediate metastable carbene species (A-1) and two concerted paths (A-2 and A-3). In the other reaction, the amino group migrates from the carbon to the silicon atom while a hydrogen atom shifts from the silicon to the carbon atom, via a double three-membered-ring transition state, forming aminomethylsilane $CH_3SiH_2NH_2$ (**3**) (reaction B).

3.1. Stationary Points. Geometries of $H_3SiCH_2NH_2$ and its rearrangement products, transition states and intermediate are given in Figure 1. The corresponding structural parameters, energies (including zero-point energy) and atomic natural charges are listed in Tables 1−3, respectively. It should be noted that atomic charge is not a quantum mechanical observable, and assigning charges to the different atoms depends on the partition scheme.

Geometries **1a** and **1b** are two stable conformers of $H_3SiCH_2NH_2$, and moreover, **1a** is slightly more stable than **1b** by 2.9 kJ/mol at the G3 level. Geometry **2a** is the only minimum of CH_3NHSiH_3 located on the CH_7NSi potential energy surface. Vibrational analysis confirms that the stationary point **IM** is a local energy minimum at both the MP2(full)/6-31G(d) and MP2(full)/6-311G(d,p) levels. MP2(full)/6-311G(d,p) natural bond orbital (NBO) analysis suggests that there is a lone pair of electrons on the carbon atom of **IM** with an occupancy of 1.956, which mainly distributes on the sp^2 hybrid orbital (33.03% and 66.90% for s and p orbital, respectively). Its H^7-C-H^8 bond angle is 105.5°, indicating that the CH_2 moiety of **IM** is a singlet state carbene. The **IM** can be viewed as a complex formed by aminosilane NH_2SiH_3 and carbene CH_2, in which the sp^3 orbital of nitrogen atom, with a lone pair of electrons, partially overlaps with the virtual p orbital of the carbon atom. The Si−N and C−N bond distances in **IM** are 0.0085 and 0.0112 nm longer than those in **2a** and **1a**, respectively. AIM (atom in molecules)[22] analysis suggests that their bond orders are 0.146 and 0.103, respectively. Minimum **3a** is the stable conformer of $CH_3SiH_2NH_2$. First-order saddle points **TS1**, **TS2**, **TS3**, **TS4** and **TS5** were verified by IRC calculations to be the transition states between **1a** and **IM**, **IM** and **2a**, **1a** and **2a**, **1a** and **2a**, and **1a** and **3a**, respectively, in which silicon atoms are all pentacoordinate. In **TS1**, the Si−C and C−N distances are respectively 0.0484 and 0.0047 nm longer than that in **1a**, and the Si−N distance is 0.0932 nm shorter than that in **1a**, but 0.0077 nm longer than that in **2a**. In **TS2**, the C−N and $N-H^9$ distances are respectively 0.0271 and 0.076 nm longer than that in **1a**, and the $C-H^9$ bond length is 0.0387 nm longer than that in **2a**. For **TS3** and **TS4**, although they are similar in the double three-membered-ring structure, their electronic differences are sig-

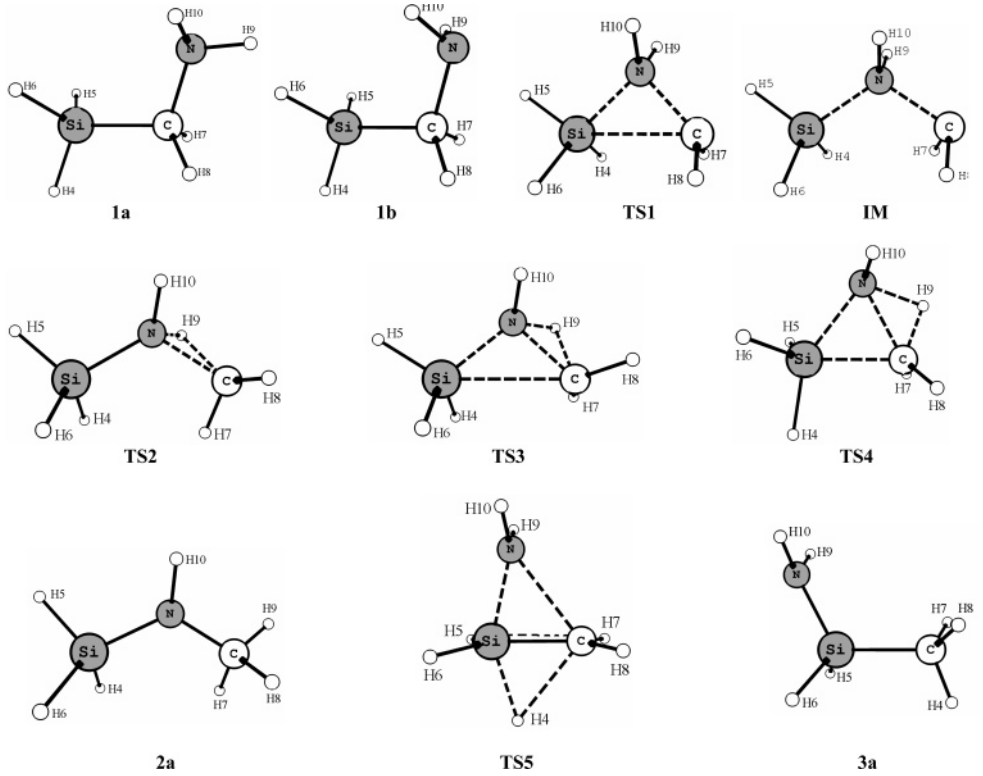

Figure 1. MP2(full)/6-311G(d,p) geometries of stationary points.

TABLE 1: MP2(full)/6-311G(d,p) Structural Parameters[a] of Stationary Points

parameter	1a	1b	TS1	IM	TS2	TS3	TS4	2a	TS5	3a
Si−C	0.1886	0.1891	0.2370	0.2820	0.2936	0.2616	0.2002	0.2791	0.1783	0.1868
Si−N	0.2735	0.2838	0.1803	0.1811	0.1766	0.1761	0.1889	0.1726	0.1866	0.1730
Si−H^4	0.1479	0.1479	0.1467	0.1464	0.1468	0.1467	0.1504	0.1476	0.1667	
Si−H^5	0.1479	0.1479	0.1504	0.1481	0.1474	0.1483	0.1476	0.1475	0.1474	0.1477
Si−H^6	0.1474	0.1479	0.1467	0.1464	0.1472	0.1468	0.1487	0.1484	0.1474	0.1485
C−N	0.1472	0.1479	0.1519	0.1584	0.1689	0.1623	0.1707	0.1458	0.2261	
C−H^4									0.204	0.1094
C−H^7	0.1101	0.1095	0.1075	0.1103	0.1097	0.1086	0.1082	0.1094	0.1091	0.1092
C−H^8	0.1095	0.1095	0.1075	0.1103	0.1094	0.1081	0.108	0.1098	0.1091	0.1094
C−H^9	0.2046			0.2106	0.148	0.1379	0.1194	0.1093	0.2884	
N−H^9	0.1014	0.1015	0.1017	0.1017	0.109	0.1154	0.1322		0.1015	0.1009
N−H^{10}	0.1014	0.1015	0.1017	0.1017	0.1012	0.1011	0.1023	0.1009	0.1015	0.1009
SiCN	108.5	114.2	49.5	36.5	32.6	41.3	60.6	31.6	53.4	33.9
H^4SiC	110.4	113.0	92.4	89.0	87.4	89.5	97.3	93.6	72.4	24.4
H^5SiC	108.8	108.7	145.4	142.4	141.1	145.9	114.6	133.3	120.9	111.2
H^6SiC	110.4	108.7	92.4	89.0	93.2	87.2	119.4	101.6	120.9	107.6
H^7CSi	110.9	110.4	93.6	80.2	69.8	100.3	102.2	84.9	122.8	110.8
H^8CSi	107.7	110.4	93.7	80.2	110.1	138.1	111.0	104.4	122.8	111.2
H^9NC	109.4	109.6	110.9	106.1	59.8	56.6	44.2	29.1	118.3	153.4
H^{10}NC	110.2	109.6	110.9	106.1	109.6	110.5	100.8	112.7	118.3	95.9
H^4SiCN	171.6	180.0	119.6	122.9	127.7	120.7	−176.8	126.2	180.0	−179.4
H^5SiCN	52.4	58.8	0.0	0.0	7.4	−3.1	76.7	2.8	93.9	117.0
H^6SiCN	−67.5	−58.8	−119.6	−122.8	−121.4	−126.5	−70.3	−126.0	−93.9	−125.9
H^7CSiH^4	44.8	58.1	1.9	−3.2	−45.1	14.6	71.5	−14.5	86.6	120.4
H^8CSiH^4	−71.4	−58.1	−122.8	−111.1	−148.1	−174.5	−63.0	−121.5	−86.6	−119.7
H^9NCSi	−69.5	57.9	−121.6	−124.6	−118.1	−134.8	−166.9	−159.5	−111.5	−33.3
H^{10}NCSi	174.1	−57.9	121.6	124.6	140.7	128.4	108.1	147.9	111.5	133.5

[a] Bond lengths are in nanometers (nm); bond and dihedral angles are in degrees.

nificant. The ∠SiNH^{9}C angles are −72.5 and −12.9°, respectively. The Si−C, C−N and N−H^9 distances are longer than those in **1a** by 0.0730, 0.0151 and 0.0140 nm for **TS3** and 0.0116, 0.0235 and 0.0308 nm for **TS4**, respectively. For **TS3** the Si−N and C−H^9 distances are longer than those in **2a** by 0.0035 and 0.0286 nm, and For **TS4** they are 0.0163 and 0.0101 nm longer. In **TS5**, the C−N and Si−H^4 distances are 0.0789 and 0.0188 nm, respectively, longer than those in **1a** and the Si−N and C−H^4 distances are 0.0136 and 0.0946 nm longer, respectively, than that in **3a**, but the Si−C distance is 0.0085 nm shorter than that in **3a**.

3.2. Mechanism of Path A-1. The IRC calculations (see Figure 2) show that the reaction of the silyl group (H_3Si−) of **1a** migrates from the carbon to the nitrogen atom while a hydrogen atom shifts from the nitrogen to the carbon atom, to form CH_3NHSiH_3, **2a**, can happen via a path involving two consecutive steps including the transition state **TS1**, intermediate metastable carbene **IM** and transition state **TS2** (Scheme 4). In

TABLE 2: Total (au) and Relative Energies[a] (kJ/mol) of Stationary Points

	G3	
stationary point	total	relative
1a	−386.296706	0.0
1b	−386.295604	2.9
TS1	−386.202284	247.9
IM	−386.210291	226.9
TS2	−386.190521	278.8
TS3	−386.170817	330.5
TS4	−386.159273	361.0
2a	−386.319628	−60.2
TS5	−386.190311	279.3
3a	−386.352352	−146.1

[a] Including ZPE corrections.

the beginning of the reaction, the silyl group rotates clockwise around the Si−C bond when observed along the Si−C direction, to an extent that hydrogen atoms on silicon and carbon atoms are nearly eclipsed. Meanwhile, the amino group rotates anticlock around the N−C bond when observed along the N−C direction, to an extent that hydrogen atoms on nitrogen and carbon atoms are nearly eclipsed. Consequently, the nitrogen atom with negative charges moves toward the silicon atom bearing positive charges. During this process, the Si−C bond gradually dissociates and C−N distance slowly lengthens, accompanied by the inversion of the CH^7H^8 group around an axis perpendicular to the SiCN plane in the direction of H^7 and H^8 moves toward the silicon atom. Before the Si−C bond fully dissociates, the C−N distance begins to shorten and reaches a minimum, leading to the transition state **TS1**. The Si−C and C−N distances increase from 0.1886 and 0.1472 nm in **1a** to 0.2370 and 0.1519 nm in **TS1**, respectively, and the positive charges on silicon atom and negative charges on carbon and nitrogen atoms increased by 0.187, 0.229 and 0.085, respectively. Once getting over the transition state **TS1**, the CH^7H^8 group reverses continuously, the C−N distance begins to increase again and the Si−C bond fully dissociates, leading to the intermediate, **IM**. During this process, the C−N and Si−C distances increase by 0.0065 and 0.0450 nm, respectively. Also the positive charges on the silicon atom and negative charges on the carbon atom decrease by 0.013 and 0.15, respectively, whereas the negative charges on the nitrogen atom increase by 0.033. Passing through the intermediate **IM**, the C−N bond lengthens continuously and reaches a maximum. Meanwhile, one of the hydrogen atoms on nitrogen, H^9, begins to leave the nitrogen atom and move toward the carbon atom, leading to the transition state **TS2**. From **IM** to **TS2**, the C−N bond length increases from 0.1584 to 0.1689 nm, whereas the C−H^9 distance decreases from 0.2106 to 0.1480 nm. The positive charges on silicon atoms and negative charges on nitrogen atoms change from 1.227 to 1.262 and −0.955 to −1.166, respectively. Getting over the transition state **TS2**, as the H^9 further approaches the carbon atom and forms the C−H^9 bond eventually, the C−N distance begins to shorten and the C−N bond forms again. As a result, the product, **2a**, is obtained. The G3 energy barriers from **1a** to **IM** (A-1a) and from **IM** to **2a** (A-1b) are 247.9 and 51.9 kJ/mol, respectively.

3.3. Mechanism of Paths A-2 and A-3. The IRC calculations (see Figure 3) show that the reaction of the silyl group of **1a** migrates from the carbon to nitrogen atom while a hydrogen atom shifts from the nitrogen to the carbon atom to form **2a** can also happen via two concerted paths passing through the transition state **TS3** or **TS4** [Scheme 4, path (A-2) and (A-3), respectively]. Similar to pathway A-1, at the beginning of the A-2 path, the silyl group rotates clockwise around the Si−C bond while the amino group rotates anticlock around the N−C bond, accompanied by the movement of the nitrogen atom toward the silicon atom. With gradually shortening of the Si−N distance, the Si−C and C−N bond lengths increase; however, the N−H^9 bond hardly changes. The C−N distance reaches a maximum before the Si−C bond fully dissociates and then begins to shorten. At the same time the N−H^9 distance begins to lengthen. As a result, the transition state **TS3** is reached. The Si−C, C−N and N−H^9 distances increase from 0.1886, 0.1472 and 0.1014 nm in reactant **1a** to 0.2616, 0.1623 and 0.1154 nm in **TS3**, respectively, and the Si−N and C−H^9 distances reduce from 0.2735 and 0.2046 nm to 0.1761 and 0.1154 nm, respectively. Meanwhile, the positive charges on silicon atom and negative charges on carbon and nitrogen atoms increase by 0.239, 0.159 and 0.287, respectively. The activation barrier for the reaction A-2 amounts to 330.5 kJ/mol. Getting over the transition state **TS3**, as the nitrogen atom further approaches the silicon atom, the Si−C bond dissociates and the C−N bond forms gradually. Meanwhile, the H^9 leaves the nitrogen atom and moves toward the carbon atom, accompanied by the rotation of the CH_3 group around an axis perpendicular to the SiNC plane in the direction of the H^9 apart from the nitrogen atom. As a result, product **2a** forms as the Si−C bond fully dissociates and the $H,^9$ silicon and nitrogen atoms fully bond to the carbon, carbon and silicon atoms, respectively.

The mechanism of path A-3 is very similar to that for A-2. The only difference is that in A-3, the silyl group does not rotate as it is in A-2. From **1a** to **TS4**, the Si−C, C−N and N−H^9 distances increase respectively from 0.1886, 0.1472 and 0.1014 nm to 0.2002, 0.1707 and 0.1322 nm, and the Si−N and C−H^9 distances reduce respectively from 0.2735 and 0.2046 nm to 0.1889 and 0.1194 nm. Meanwhile, the positive charges on silicon atom and negative charges on carbon and nitrogen atoms increase by 0.174, 0.251 and 0.054, respectively. Compared to those for A-1a and A-2, the activation energy of A-3 is 361.0 kJ/mol, 113.1 and 30.5 kJ/mol higher.

3.4. Mechanism of Reaction B. The IRC calculations in Figure 2 show that the reaction forming aminomethylsilane CH_3-SiH_2NH_2 (**3**), in which the amino group of **1a** migrates from the carbon to the silicon atom while a hydrogen atom shifts from the silicon atom (Scheme 4, path B), is a concerted reaction passing through the double three-member-ring transition state **TS5**, where the silicon atom is pentacoordinate. The reaction

TABLE 3: MP2(full)/6-311G(d,p) Atomic Natural Charges of Stationary Points

stationary point	Si	C	N	H^4	H^5	H^6	H^7	H^8	H^9	H^{10}
1a	1.053	−0.551	−0.837	−0.225	−0.225	−0.211	0.155	0.178	0.329	0.334
TS1	1.240	−0.780	−0.922	−0.203	−0.292	−0.203	0.172	0.172	0.408	0.408
IM	1.227	−0.630	−0.955	−0.201	−0.234	−0.201	0.092	0.092	0.405	0.405
TS2	1.262	−0.590	−1.166	−0.214	−0.229	−0.221	0.115	0.129	0.515	0.402
TS3	1.292	−0.710	−1.124	−0.220	−0.254	−0.209	0.167	0.170	0.490	0.396
TS4	1.227	−0.802	−0.891	−0.294	−0.221	−0.241	0.242	0.226	0.409	0.345
2a	1.276	−0.246	−1.117	−0.241	−0.235	−0.258	0.155	0.136	0.156	0.373
TS5	1.209	−0.324	−1.256	−0.313	−0.208	−0.208	0.182	0.182	0.368	0.368
3a	1.479	−1.025	−1.291	0.202	−0.250	−0.270	0.206	0.199	0.376	0.373

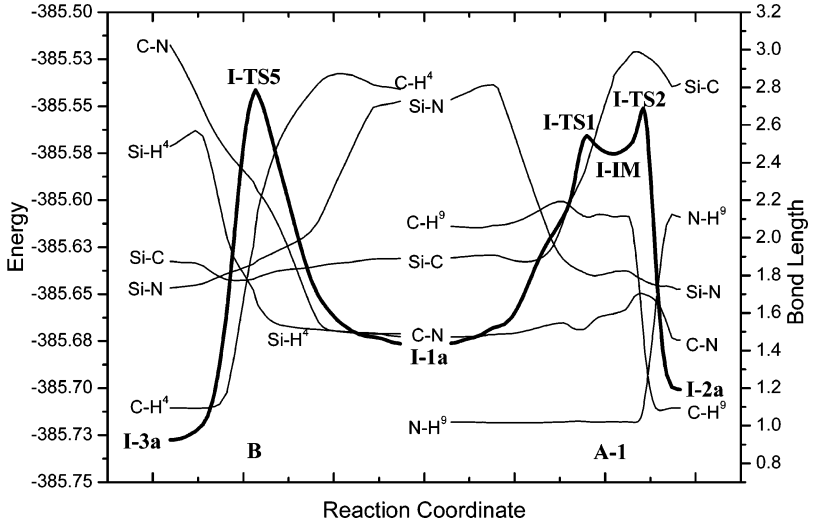

Figure 2. Energy and bond length vs reaction coordinate at the MP2(full)/6-31G(d) levels.

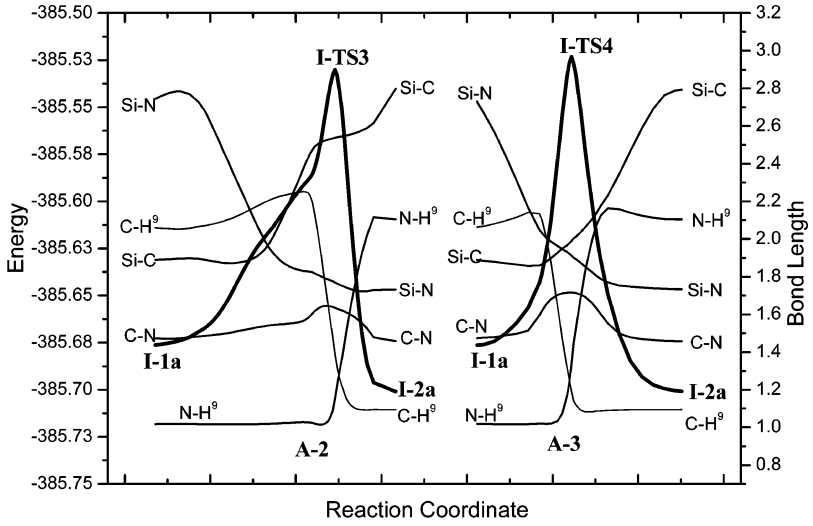

Figure 3. Energy and bond length vs reaction coordinate at the MP2(full)/6-31G(d) levels.

begins as the amino group of reactant **1a** moves toward the silicon atom accompanying the rotation of the amino group around the N−C bond in the direction of anticlockwise. It can be seen from Figure 2 that at the beginning of the reaction, the C−N and Si−H^4 distances lengthen slowly. As the amino group further approaches the silicon atom, the distances of the C−N and Si−H^4 lengthen rapidly, leading to the transition state **TS5**. From **1a** to **TS5**, the Si−N distance reduces from 0.2735 to 0.1866 nm, and the C−N and Si−H^4 distances increase respectively from 0.1472 and 0.1479 nm to 0.2261 and 0.1667 nm. The positive charges on the silicon atom and negative charges on the nitrogen atom increase by 0.156 and 0.419, respectively, and negative charges on the carbon atom decrease by 0.227. The activation barrier for the reaction is 279.3 kJ/mol, 31.4 kJ/mol higher than that of path A-1. Once getting over the transition structure, the amino group continuously approaches the silicon atom; meanwhile, the H^4 departs from the silicon and moves toward the carbon atom. As a result, the product **3a** forms when the amino group attaches to the silicon atom, the H^4 attaches to the carbon atom and the Si−H^4 bond fully dissociates.

3.5. Kinetic and Thermodynamic Analyses. Kinetic and thermodynamic analyses may further illustrate the feasibility and likelihood of such reactions. There are many reports on the theoretical research of kinetic properties.[11,23−29] We carried out the kinetic and thermodynamic calculations for rearrangements A and B based on the MP2(full)/6-311G(d,p) optimized parameters, vibrational frequencies (scaled by 0.949[30]) (see Supporting Information) and G3 energies, in conventional transition-state theory (TST) with Wigner tunneling approximation over a temperature range from 400 to 1800 K. For path A-1, the chemical reaction can be expressed as

$$1 \underset{k_{-(A-1a)}}{\overset{k_{A-1a}}{\rightleftharpoons}} \mathrm{Im} \xrightarrow{k_{A-1b}} 2$$

where k_{A-1a}, k_{A-1b} and $k_{-(A-1a)}$ are the microscopic rate constants. Using the steady-state approximation, the whole rate constant k_{A-1} is given by

$$k_{A-1} = \frac{k_{A-1a} \times k_{A-1b}}{k_{(A-1a)} + k_{A-1b}}$$

The results are listed in Tables 4 and 5.

The following points can be found from the data in Tables 4 and 5: (1) for all paths under study, the tunneling effects are too small to change the order of magnitude of rate constants; (2) the reaction rate constants of step A-1a are much less than

TABLE 4: TST and TST/W Rate Constants k (s^{-1})

	TST							TST/W					
T (K)	k_{A-1a}	$k_{-(A-1a)}$	k_{A-1b}	k_{A-1}	k_{A-2}	k_{A-3}	k_B	k_{A-1b}	k_{A-1}	k_{A-2}	k_{A-3}	k_B	k_{A-1}/k_B
400	3.8E−19	5.9E+10	2.6E+08	1.7E−21	2.7E−28	8.6E−33	3.7E−22	5.3E+08	3.4E−21	6.3E−28	2.1E−32	5.8E−22	5.8
500	9.3E−13	2.0E+11	3.5E+09	1.6E−14	5.2E−20	9.7E−24	3.1E−15	5.8E+09	2.6E−14	9.6E−20	1.9E−23	4.2E−15	6.2
600	1.7E−08	4.6E+11	2.0E+10	7.1E−10	1.8E−14	1.1E−17	1.3E−10	2.9E+10	1.0E−09	2.9E−14	1.8E−17	1.7E−10	5.9
700	2.0E−05	8.5E+11	7.3E+10	1.6E−06	1.7E−10	2.3E−13	2.9E−07	9.6E+10	2.0E−06	2.4E−10	3.4E−13	3.4E−07	6.0
800	3.9E−03	1.3E+12	1.9E+11	5.0E−04	1.6E−07	4.0E−10	9.2E−05	2.4E+11	6.1E−04	2.1E−07	5.5E−10	1.1E−04	5.5
900	2.4E−01	1.9E+12	4.0E+11	4.2E−02	3.4E−05	1.4E−07	8.4E−03	4.8E+11	4.8E−02	4.3E−05	1.7E−07	9.4E−03	5.1
1000	6.4E+00	2.6E+12	7.4E+11	1.4E+00	2.5E−03	1.4E−05	3.1E−01	8.6E+11	1.6E+00	3.0E−03	1.8E−05	3.4E−01	4.7
1100	9.6E+01	3.2E+12	1.2E+12	2.6E+01	8.3E−02	6.5E−04	6.1E+00	1.4E+12	2.9E+01	9.8E−02	7.8E−04	6.5E+00	4.5
1200	9.1E+02	3.9E+12	1.9E+12	3.0E+02	1.6E+00	1.6E−02	7.2E+01	2.1E+12	3.2E+02	1.8E+00	1.8E−02	7.7E+01	4.1
1300	6.1E+03	4.7E+12	2.7E+12	2.2E+03	1.9E+01	2.3E−01	5.9E+02	2.9E+12	2.3E+03	2.1E+01	2.6E−01	6.3E+02	3.7
1400	3.1E+04	5.4E+12	3.6E+12	1.2E+04	1.6E+02	2.3E+00	3.6E+03	3.9E+12	1.3E+04	1.8E+02	2.6E+00	3.8E+03	3.4
1500	1.3E+05	6.1E+12	4.8E+12	5.7E+04	1.0E+03	1.7E+01	1.7E+04	5.1E+12	5.9E+04	1.1E+03	1.9E+01	1.8E+04	3.3
1600	4.5E+05	6.8E+12	6.0E+12	2.1E+05	5.2E+03	9.9E+01	6.8E+04	6.4E+12	2.2E+05	5.6E+03	1.1E+02	7.1E+04	3.1
1700	1.3E+06	7.5E+12	7.5E+12	6.5E+05	2.2E+04	4.7E+02	2.3E+05	7.9E+12	6.7E+05	2.3E+04	5.0E+02	2.4E+05	2.8
1800	3.5E+06	8.2E+12	9.0E+12	1.8E+06	7.8E+04	1.8E+03	6.7E+05	9.4E+12	1.9E+06	8.3E+04	2.0E+03	6.9E+05	2.7

TABLE 5: Equilibrium Constants K, Changes of Activation Entropy $\Delta S^{\ddagger}$ (J/K), Free Energy ΔG (kJ/mol) and Enthalpy ΔH (kJ/mol)

T (K)	$\Delta S^{\ddagger}_{A-1a}$	$\Delta S^{\ddagger}_{A-1b}$	$\Delta S^{\ddagger}_{A-2}$	$\Delta S^{\ddagger}_{A-3}$	$\Delta S^{\ddagger}_{B}$	K_A	K_B	ΔG_A	ΔG_B	ΔH_A	ΔH_B
400	−5.21	6.43	3.95	−9.95	−3.99	9.0E+08	2.4E+19	−62.1	−35.5	−59.97	−143.85
500	−5.62	6.08	4.32	−10.17	−2.57	3.0E+06	4.2E+15	−62.6	−35.8	−60.14	−143.28
600	−6.13	5.60	4.44	−10.38	−1.65	2.9E+05	1.3E+13	−63.0	−36.1	−60.31	−142.86
700	−6.71	5.07	4.38	−10.62	−1.13	5.4E+04	2.2E+11	−63.5	−36.4	−60.45	−142.60
800	−7.33	4.54	4.21	−10.89	−0.90	1.7E+04	1.0E+10	−63.9	−36.8	−60.55	−142.45
900	−7.97	4.01	3.97	−11.18	−0.87	6.5E+03	9.5E+08	−64.3	−37.1	−60.63	−142.39
1000	−8.61	3.51	3.68	−11.48	−0.97	2.9E+03	1.4E+08	−64.7	−37.5	−60.69	−142.39
1100	−9.22	3.02	3.37	−11.80	−1.17	1.6E+03	2.9E+07	−65.1	−37.8	−60.73	−142.43
1200	−9.82	2.55	3.04	−12.12	−1.42	9.5E+02	8.1E+06	−65.5	−38.1	−60.75	−142.51
1300	−10.39	2.10	2.71	−12.45	−1.71	5.5E+02	2.7E+06	−65.9	−38.5	−60.76	−142.60
1400	−10.94	1.67	2.36	−12.78	−2.03	4.0E+02	1.0E+06	−66.3	−38.8	−60.77	−142.70
1500	−11.46	1.25	2.02	−13.11	−2.35	2.8E+02	4.6E+05	−66.7	−39.2	−60.76	−142.80
1600	−11.95	0.84	1.68	−13.43	−2.69	2.2E+02	2.2E+05	−67.1	−39.5	−60.76	−142.91
1700	−12.43	0.45	1.35	−13.76	−3.02	1.6E+02	1.2E+05	−67.5	−39.8	−60.75	−143.01
1800	−12.88	0.08	1.02	−14.07	−3.35	1.3E+02	6.8E+04	−67.9	−40.2	−60.74	−143.12

those of step A-1b, but much larger than those of paths A-2 and A-3. This indicates that A-1a is the rate-determining step of path A-1, and that path A-1 will dominate among the three paths of reaction A; (3) within the temperature range studied, the rate constants of reaction A are larger than those of reaction B at the same temperature, suggesting that the silyl group migration, reaction A, is favored kinetically over the hydroxyl migration, reaction B; (4) the ratios of rate constants of two reactions (k_{A-1}/k_B) are less than 1000 when the temperature is higher than 400 K and decrease as the temperature increases. On the contrary, the equilibrium constants of reaction B are larger than those of reaction A over the whole temperature range, and also, their ratios between reaction A and B decrease as the temperature inceases. Because they can hardly happen when the temperature is lower than 400 K it is reasonable to believe that the two reactions are competitive over the whole studied temperature range; (5) the negative ΔG values indicate that the two reactions are spontaneous. With increasing temperature, the ΔG values of both reaction **A** and **B** increase slightly; (6) for all paths under study, the changes of activation entropy ($\Delta S^{\ddagger}$) decrease over the whole studied temperatures range and are in the sequence of $\Delta S^{\ddagger}_{A-2} > \Delta S^{\ddagger}_{B} > \Delta S^{\ddagger}_{A-1a} > \Delta S^{\ddagger}_{A-3}$.

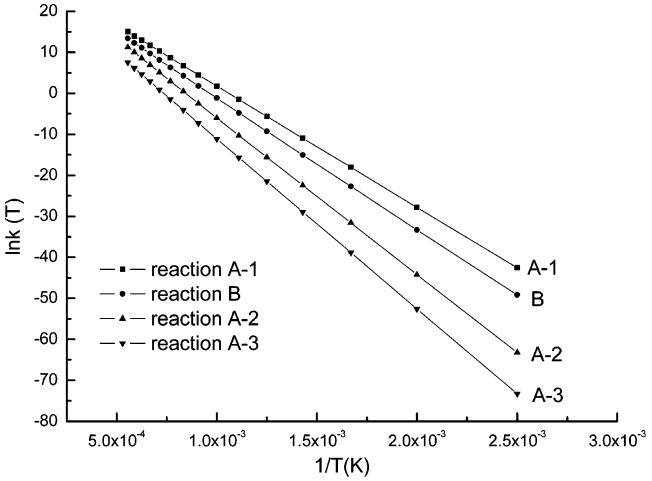

Figure 4. ln $k(T)_{TST/W}$ against $1/T$(K).

Figure 4 shows the rate constants against temperature for reactions A and B and path A-2 and A-3 over a temperature range from 400 to 1800 K. The relationship between rate constant $k(T)$ and temperature T exhibits typical Arrhenius behavior according to the following equations (in units of s^{-1}):

$$k(T) = 8.0 \times 10^{13} \exp\left(\frac{-262.7 \times 10^3}{8.314T}\right) \quad \text{for path A-1}$$

$$k(T) = 1.5 \times 10^{14} \exp\left(\frac{-320.2 \times 10^3}{8.314T}\right) \quad \text{for path A-2}$$

$$k(T) = 2.8 \times 10^{13} \exp\left(\frac{-350.4 \times 10^3}{8.314T}\right) \quad \text{for path A-3}$$

$$k(T) = 1.5 \times 10^{13} \exp\left(\frac{-277.6 \times 10^3}{8.314T}\right) \quad \text{for path B}$$

It can be seen from the four equations that the preexponential factors of path A-2, A-1,B and A-3 are 1.5×10^{14}, 8.0×10^{13}, 7.5×10^{13} and 2.8×10^{13}, respectively, in the same sequence

with their changes of activation entropies ($S^{\ddagger}$). This is in agreement with the effect of $S^{\ddagger}$ on preexponential factor.

4. Conclusions

On the basis of our calculations, we may draw the following conclusions. (1) Two dyotropic rearrangement reactions can occur when (aminomethyl)silane is heated. One is a silyl migration reaction, in which the silyl group migrates from the carbon to the nitrogen atom while a hydrogen atom shifts from the nitrogen to the carbon atom, forming (methylamino)silane (reaction A). This reaction can proceed via three paths: a path involving two consecutive steps with two transition states and one intermediate metastable carbene species (A-1); and two concerted paths (A-2 and A-3). The activation energies are 247.9, 330.5 and 361.0 kJ/mol for path A-1, A-2 and A-3, respectively. The other is an amino group migration reaction, in which the migration of the amino group from the carbon to the silicon atom is coupled to a simultaneous migration of a hydrogen atom from the silicon to the carbon atom, via a double three-membered ring transition state, forming aminomethylsilane (reaction B). The activation energy of reaction B is 279.3 kJ/mol. (2) Thermodynamic and kinetic analyses indicate that among the three paths of reaction A, path A-1 is the dominant one within the studied temperature range. (3) Within the studied temperature range, the two reactions are competitive but the silyl group migration reaction is favored over the amino group migration reaction.

Studies made by Claes and Deleuze[31] have shown that with the rising of temperatures, entropy contributions to the activation energies of thermal rearrangement reactions are significant and favor direct radical dissociation pathways. With regard to the extremely high energy barriers and limited rate constants of the two reactions, temperatures larger than 700 K would be required for obtaining rate constants larger than 10^{-3} s and monitoring such reactions on a daily scale. At such temperatures, in view of more favorable entropy effects, radical dissociation pathways are expected to be very competitive. These pathways should be investigated in detail in further theoretical studies.

Acknowledgment. We thank Professor Donald G. Truhlar for providing the POLYRATE 9.0 program and Doctor Jun Zhang of Shandong University and Yan Zhao of the University of Minnesota for their help in using the POLYRATE. This work was supported by the National Natural Science Foundation of China, the Natural Science Foundation of Shandong Province, Reward Funds for the Outstanding Young by Shandong University, Foundation for University Key Teacher by the Ministry of Education and Scientific Research Starting Foundation for the Return Overseas Chinese Scholar by the Ministry of Education.

Supporting Information Available: Energies of stationary points at the MP2(full)/6-31(d) and MP2(full)/6-311G(d,p) levels. Vibrational frequencies. This material is available free of charge via the Internet at http://www.pubs.acs.org.

References and Notes

(1) Brook, A. G.; Duff, J. M. *J. Am. Chem. Soc.* **1974**, *96*, 4692−4693.

(2) Harris, Joanna M.; Walton, John C. *J. Chem. Soc., Perkin Trans. 2* **1993**, *2119*.

(3) Harris, J. M.; Macinnes, I.; Walton, J. C.; Maillard, B. *J. Organomet. Chem.* **1991**, *403*, C25.

(4) Roberts, Brian P.; Vazquez-Persaud, Anthony R. *J. Chem. Soc., Perkin Trans. 2* **1995**, 1087.

(5) Carl Schiesser, H.; Styles, Michelle L. *J. Chem. Soc., Perkin Trans. 2* **1997**, *2335*.

(6) (a) Speier J. L.; Roth, C. A.; Ryan, R. W. *J Org. Chem.* **1971**, *36*, 3120. (b) Burns, G. T.; Decker, G. T.; Roy, A. K. U.S. Patent 5290901 to Dow Corning, 1994. (c) Feng, S. Y.; Zhang, J.; Li, M. J.; Zhu, Q. Z. *Organosilicon Polymers and Their Applications*; Chemical Industry Press: Beijing, P. R. China, 2004; pp 47−50 and 241−246.

(7) Møller, C.; Plesset, M. *Phys. Rev.* **1934**, *46*, 618−622.

(8) Curtiss, L. A.; Raghavachari, K.; Redfern, P. C.; Rassolov, V.; Pople, J. A. *J. Chem Phys.* **1998**, *109*, 7764.

(9) (a) Carpenter, J. E.; Weinhold, F. *J. Mol. Struct. (THEOCHEM).* **1988**, *169*, 41. (b) Carpenter, J. E. Ph.D. Thesis, University of Wisconsin, Madison, WI, 1987. (c) Foster, J. P.; Weinhold, F. *J. Am. Chem. Soc.* **1980**, *102*, 7211. (d) Reed, A. E.; Weinhold, F. *J. Chem. Phys.* **1983**, *78*, 4066. (e) Reed, A. E.; Weinhold, F. *J. Chem. Phys.* **1983**, 1736. (f) Reed, A. E.; Weinstock, R. B.; Weinhold, F. *J. Chem. Phys.* **1985**, *83*, 735. (g) Reed, A. E.; Curtiss, L. A.; Weinhold, F. *Chem. Rev.* **1988**, *88*, 899.

(10) Frisch, M. J.; Trucks, G. W.; Schlegel, H. B.; Scuseria, G. E.; Robb, M. A.; Cheeseman; Zakrzewski, V. G.; Montgomery, J. A., Jr.; Stratmann, R. E.; Burant, J. C.; Dapprich, S.; Millam, J. M.; Daniels, A. D.; Kudin, K. N.; Strain, M. C.; Farkas, O.; Tomasi, J.; Barone, V.; Cossi, M.; Cammi, R.; Mennucci, B.; Pomelli, C.; Adamo, C.; Clifford, S.; Ochterski, J.; Petersson, G. A.; Ayala, P. Y.; Cui, Q.; Morokuma, K.; Malick, D. K.; Rabuck, A. D.; Raghavachari, K.; Foresman, J. B.; Cioslowski, J.; Ortiz, J. V.; Baboul, A. G.; Stefanov, B. B.; Liu, G.; Liashenko, A.; Piskorz, P.; Komaromi, I.; Gomperts, R.; Martin, R. L.; Fox, D. J.; Keith, T.; Al-Laham, M. A.; Peng, C. Y.; Nanayakkara, A.; Challacombe, M.; Gill, P. M. W.; Johnson, B.; Chen, W.; Wong, M. W.; Andres, J. L.; Gonzalez, C.; Head-Gordon, M.; Replogle, E. S.; Pople, J. A. *Gaussian 03*, revision C.02; Gaussian, Inc.: Wallingford, CT, 2004.

(11) Ju, G.; Feng, D.; Deng, C. *Acta Chim. Sinica* **1985**, *43*, 680.

(12) Eyring, H. *J. Chem. Phys.* **1935**, *3*, 492.

(13) Evans, M. G.; Polanyi, M. *Trans. Faraday Soc.* **1935**, *31*, 875.

(14) Evans, M. G.; Polanyi, M. *Trans. Faraday Soc.* **1937**, *33*, 448.

(15) Laidler, K. J.; King, M. C. *J. Phys. Chem.* **1983**, *87*, 2657.

(16) Truhlar, D. G.; Hase, W. L.; Hynes, J. T. *J. Phys. Chem.* **1983**, *87*, 2664.

(17) Gilbert, R. G.; Smith, S. C. Theory of Unimolecular and Recombination Reactions; Blackwell: Oxford, U.K., 1990.

(18) Chuang, Yao-Yuan; Truhlar, Donald G. *J. Chem. Phys.* **2000**, *112*, 1221−1228.

(19) Hirschfelder, J. O.; Wigner, E. *J. Chem. Phys.* **1937**, *7*, 616.

(20) Steckler, R.; Chuang, Y. Y.; Fast, P. L.; Corchade, J. C.; Coitino, E. L.; Hu, W. P.; Lynch, G. C.; Nguyen, K.; Jackells, C. F.; Gu, M. Z.; Rossi, I.; Clayton, S.; Melissas, V.; Garrett, B. C.; Isaacson, A. D.; Truhlar, D. G. *POLYRATE*, 9.0 version; University of Minnesota: Minneapolis, MN, 2002.

(21) Reetz, Manfred T. *Angew. Chem. Int. Ed.* **1972**, *11*, 129−131.

(22) Bader, R. F. W. *Atoms in Molecules*: *A Quantum Theory*; Oxford University Press: Oxford, U.K., 1990.

(23) Baldrige, K. K.; Gordor, M. S.; Steckler, R.; Truhlar, D. G. *J. Phys. Chem.* **1989**, *93*, 5107.

(24) Gonzalez-Lafont, A.; Truong, T. N.; Truhlar, D. G. *J. Chem. Phys.*, **1991**, *95*, 8875.

(25) Garrett B. C.; Truhlar, D. G. *J. Phys. Chem.* **1979**, *83*, 1052.

(26) Sumathi, R.; Green, William H., Jr. *Theor. Chem. Acc.* **2002**, *108*, 187−213.

(27) Sumathi, R.; Green, William H., Jr. *J. Phys. Chem. A* **2001**, *105*, 6910−6925.

(28) Sumathi, R.; Green, William H., Jr. *PhysChemChemPhys* **2003**, *5*, 3402−3417.

(29) VAN Speybroeck, V.; Van Neek, D.; Waroquier, M. *J. Phys. Chem. A* **2000**, *104* (46), 10939−10950.

(30) "Precomputed vibrational scaling factors", online available at http://srdata.nist.gov/cccbdb/vibscalejust.asp, Computational Chemistry Comparison and Benchmark Database (CCCBDB), released by National Institute of Standards and Technology (http://www.nist.gov).

(31) Claes, L.; Francüois, J.-P.; Deleuze, M. S. *J. Am. Chem. Soc.* **2003**, *125*, 7129−7138.